Solid-state Metal Additive Manufacturing Using Friction Surfacing

By

Hemant Agiwal

A report submitted at the completion of the project
through the Austrian Marshall Plan Foundation Scholarship
at the
IFT, TU Wien
2022

Date of final submission: 30/11/22

The project report is approved by the following members at the home and host university:

Frank Pfefferkorn, Professor, UW-Madison &
Austrian Marshall Plan Foundation Professor (TU Wien)

Univ. Prof. Dr. Friedrich Bleicher, TU Wien

Assistant Prof. Stephan Krall, IFT, TU Wien

Project overview:

TITLE OF RESEARCH PROJECT: Solid-state Metal Additive Manufacturing Using Friction Surfacing

SUPERVISOR AT HOME UNIVERSITY: Prof. Frank E. Pfefferkorn, Department of Mechanical Engineering, University of Wisconsin-Madison (UW-Madison)

SUPERVISOR AT HOST UNIVERSITY: Univ. Prof. Dr. Friedrich Bleicher, Assistant Prof. Stephan Krall, IFT, TU Wien

RESEARCH TEAM AT HOST UNIVERSITY: Christian Baumann, Thomas Koch

SHORT DESCRIPTION OF RESEARCH AGENDA: This research explores and evaluates friction surfacing as a solid-state metal additive process for building 3D structures and repairing damaged parts. In other words, depositing metal without the need to melt

RESEARCH GOALS: Following are the general goals that were aimed for completion in close coordination with TU Wien colleagues through this research visit.

Goal 1: Use knowledge gained from 2021 experiments to achieve uniform multilayer friction surfaced coatings using stainless steel 304L. (Completed)

From the data collected in the previous experiments, a new set of experiments were designed with a variety of materials to gain more insights into the role of processing parameters on the deposition quality and properties. The methodology developed and results have been presented in section A.1

Goal 2: Perform mechanical characterization and microstructural examination of deposited coatings. (Completed)

Tensile tests and chemical etching was performed for friction surfaced coatings at TU Wien, and the results are presented in section A.1.

Goal 3: Explore friction surfacing for repairing regions of damaged structures. (Completed)

Several demonstrations were performed at IFT, TU Wien partnering with industrial collaborators to spark further discussion for the potential use of the technology as a repair method. The discussions were positive, and future collaborations will continue to explore the application more.

A.1 Dimensionless numbers for predicting process parameter boundaries in friction surfacing

Abstract

This study presents two dimensionless numbers for parameter selection to achieve consolidated bonding during the friction surfacing process. The dimensionless numbers are formulated using the input process parameters, viz., spindle speed, rod diameter, traverse and axial feed rates, and the thermal properties of the consumable rod material. Friction surfacing was performed using aluminum 6060 alloys on the substrate of the same material. The heat flux and axial pressure are plotted against the dimensionless numbers, and regimens of processing conditions that produce sound bonding conditions are identified. The dimensionless numbers are verified for friction surfacing performed with a 304L stainless steel rod and substrate.

A.1.1 Introduction

Friction surfacing (FS) is an emerging solid-state deposition process belonging to the family of 'third-body region' based manufacturing processes such as friction stir welding, friction welding, etc. Figure 1 shows the schematic illustration of FS. During friction surfacing, a rotating consumable rod is pressed against a stationary substrate under an applied axial load. The friction contact leads to the generation of a viscoplastic boundary between the rod and the substrate that plastically deforms the rod. The plastically deformed consumable rod is traversed over a substrate to provide a dense uniform coating. Figure 1b shows the thermomechanical events occurring during FS. As the unconstrained rotating rod is traversed across the substrate, material at the frictional interface either becomes a flash or will roll onto the substrate [1].

During FS, the consumable rod's rotation speed, traverse feed rate, axial force or axial feed rate, consumable rod diameter, and tilt angle are the major processing parameters affecting the physics and, therefore, the properties of the deposit. The effect of these individual parameters on the deposition morphology, efficiency, mechanical properties, and microstructure has been discussed by Gandra et al. [2]. The correct selection of these parameters becomes crucial from the performance standpoint. Vitanov et al. [3] used surface response methodology to identify relationships between input variables and process signatures, such as strength and torque. The authors reported trends for a select combination of parameters on the performance of the coating. Voutchkov et al. [4] used artificial intelligence to train mathematical models with the coating appearance, temperature, process forces, and bond strength. They used a 'neural network' based model to predict the performance of the deposits for a select combination of process parameters. The literature consists of numerous publications discussing the optimum processing windows for FS of various materials

experiment. The bonding capabilities of individual coatings were qualitatively analyzed by a peel-off testing method. The coatings were impacted laterally near the interface by a chisel that was hit with a hammer. If the coating peeled off, it was labeled as 'unacceptable', and all others were labeled 'acceptable.' For selected experimental conditions, the bonding strength of the coatings was quantified in terms of the tensile properties. Room temperature tensile tests were performed on a universal testing machine (MTS®, Sintech, USA) load frame with a 50 kN load cell and 2.20 mV/V sensitivity per the ASTM E8 standard. Tests were carried out at a constant crosshead rate of 5 mm/min (strain rate of 0.1 s^{-1}), and data were collected at 10 Hz. The methods were validated on a different material using stainless steel 304L consumable rods and substrate at UW-Madison, using a similar 3-axis CNC milling machine (HAAS TM-1). The experimental parameters are listed in Table 1.

Table 1. Friction surfacing parameters used in this study

	Aluminum 6060	Stainless steel 304L
Spindle speed, N	4,000 - 7,000 RPM	1,500-20,000 RPM
Consumable rod diameter, (2r)	10, 12, and 15 mm	4.76, 9.5, 12.75 mm
Lateral traverse feed rate, (V_x)	800-2,000 mm/min	90-150 mm/ min
Axial feed rate, (V_z)	440-1,100 mm/min	50-85 mm/min
Feed ratio, V_z/V_x	0.55	0.55
Initial plunge	1 mm	1 mm
Initial plunge rate	20 mm/min	20 mm/min
Dwell at the end of the plunge	0.25 seconds	0.25 seconds

A.1.3 Dimensionless numbers

Throughout the literature, obtaining the right set of process parameters for any application, rod material, and machine specifications is still not consolidated. In this study, two dimensionless numbers based on the input parameters (spindle speed, traverse speeds), material properties, and rod diameter have been used. These dimensionless numbers were created using the Buckingham-Pi theorem. The relevant physical properties of the friction surfacing process are listed in table 2.

Table 2: Physical properties used in this study for dimensional analyses

	Physical quantity	**Unit**	**Dimension [M L T θ]**
Geometric variable	Consumable rod radius (r)	mm	[0 1 0 0]
Process variables	Spindle speed (N)	Rad/s	[0 0 -1 0]
	Traverse feed rate (V_x)	mm/min	[0 1 -1 0]
	Initial temperature (T_o)	K	[0 0 0 1]
Material properties	Melting point (T_m)	K	[0 0 0 1]
	Thermal conductivity (k)	W/m-s	[1 1 -3 -1]
	Specific heat capacity (c)	J/kg-K	[0 2 -2 -1]
	Density (ρ)	kg/m^3	[1 -3 0 0]
	Yield strength (σ_y)	MPa	[1 -1 -2 0]

This dimensionless number τ_1 can be modified as:

$$\theta = \frac{T_m - T_o}{T_m} \qquad (6)$$

Using these previously presented numbers two numbers were created, the first dimensionless number is created by combining τ_2, τ_3, τ_4, and θ.

$$\frac{\tau_3 \tau_4}{\tau_2 \theta} = \frac{\rho C_p V_x^2 (T_m - T_o)}{k N t_o} \qquad (7)$$

Some additional transformations in this equation:

$$\text{Thermal diffusivity, } \alpha = \frac{k}{\rho c} \qquad (8)$$

Using equation (5),

$$V_x = \frac{r N}{\tau_5} \qquad (9)$$

Thus, using equations (8) and (9):

$$\boldsymbol{\pi_1 = \frac{N r^2}{\alpha \theta}} \qquad \textbf{(10)}$$

The second dimensionless number is also created using τ_2, τ_3, and τ_4.

$$\frac{\tau_3 \tau_4}{\tau_2} = \frac{\rho C_p V_x^2}{k N} \qquad (11)$$

Using equation (5),

$$N = \frac{V_x}{\tau_5 r} \qquad (12)$$

Using equation (8), (11) and (12):

$$\boldsymbol{\pi_2 = \frac{V_x r}{\alpha} = Pe\ (Peclet\ number)} \qquad \textbf{(13)}$$

The first number (π_1) is calculated using the spindle speed (N, rad/s), consumable rod radius (r, m), thermal diffusivity of rod material (α, m^2/s), and dimensionless temperature of the rod (θ), calculated using the rod's solidus (T_m) and initial (T_o) temperature. The numerator can also be represented as the product of tangential velocity ($V_a = N r$) and radius of the rod (r); thus, the numerator can now be seen as the moment of strain rate. Since the outer periphery of the rod has the highest strain rate, it will have the highest strain energy. Strain energy translates to the plastic work done during the

A.1.4 Results

A.1.4.1 Deposition morphology and bond characterization

Figure 2 (a-b) shows the coating and consumable rod from friction surfacing experiments performed. All depositions show similarities in deposition appearance and the mushrooming flash on the consumable rods. A typical cross-sectional appearance of FSed coating is shown in Figure 2c. These cross-sections are consistent for all specimens throughout the study. For each coating cross-section, the total width and thickness of the coating were measured. The diameter of the cylindrical flash around the tool was also measured. The deposition morphology measured axial force and bonding characteristics for all experiments have been summarized in Appendix. The bond quality for FSed coatings was characterized using peel-off tests. The coatings were classified as acceptable or unacceptable based on the results after the peel-off tests. Figure 3 (a-b) shows unacceptable and acceptable FSed coatings from the peel-off tests.

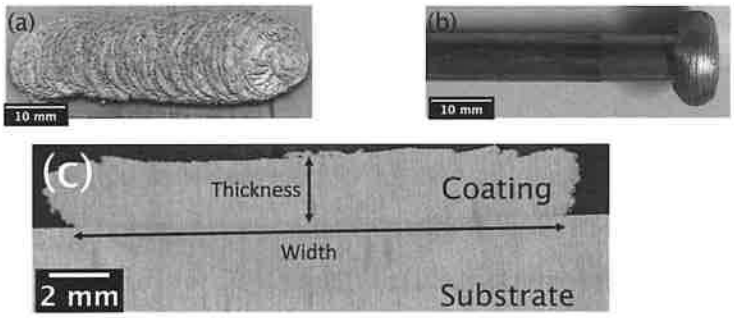

Figure 2. (a) FS coating, (b) consumable rod, and (c) cross-sectional view of the coating

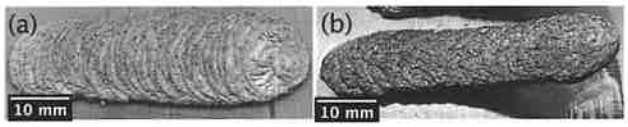

Figure 3. Results from peel-off test (a) acceptable bond and (b) unacceptable bond

A.1.4.2 Mapping of dimensionless numbers on process physics

The normalized pressure calculated across all experiments from the recorded force has been plotted against the two dimensionless numbers in Figure 5. Using the pressure values, an extrapolated pressure contour field has been drawn to highlight the regions with various ranges of normalized pressure. Each experiment has been represented by markers for an acceptable or unacceptable bond, determined by the peel-off tests. For successful diffusion bonding during friction surfacing, the processing conditions should generate sufficient pressure and heat. From the pressure field, it can be directly observed that a higher pressure can be correlated with improved bonding. Based on the

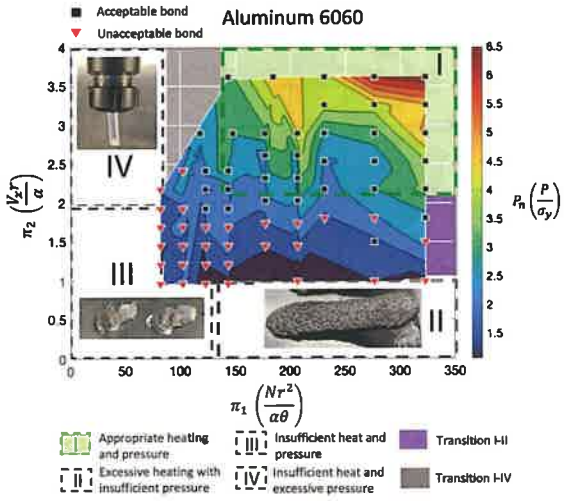

Figure 5. Variation of normalized pressure with dimensionless numbers

A.1.4.3 Heat flux variation

Several analytical equations and expressions have been used in this study to understand the dynamics of the friction surfacing process and calculate the heat flux.

A.2.1 Tangential velocity

To understand the interaction of rod diameter and rotation speed, the tangential velocity (V_a) in m/s of the outer surface of the rod (Fig. 6a) is calculated.

$$V_a = N\,r \qquad (14)$$

Where, $N$is the rotation speed of the rod in rad/s, and r_o is the radius of the rod. Through the various combinations of rod diameter and rotation speed, a well-distributed dataset of V_a (1.5 m/s - 5 m/s).

A.2.2 Radius of contact

The term 'radius of contact' or 'real rotational contact area' was first introduced by Fukakusa et al. The authors postulated that only the central part of the rod gets deposited into the coating, hence is in contact with the coating, and the periphery of the rod rolls out as a flash. The radius of this central region getting deposited, i.e., the radius of contact, r_c, can be calculated using a mass balance based on the deposition geometry and process parameters (Figure 6).

$$r_c = \sqrt{\frac{t.w.V_x}{\pi.V_z}} \qquad (15)$$

where, r_c represents the radius of contact, t is the thickness of the coating, w is the width of the coating, V_x is the traverse feed rate and V_z is the axial feed rate.

For this study, the focus is on understanding the relative impact of processing conditions on bonding characteristics and, therefore, the maximum heat flux at $(r = r_c)$ is calculated. Secondly, since we want to focus on the steady-state deposition phase during friction surfacing, 80% of the solidus temperature of the rod is assumed during deposition $(T = 0.8\,T_m)$. This assumption is validated within the literature. Thus, the final expression for maximum heat flux, $q''_{t,max}$ is as follows:

$$q''_{t,max} = \frac{N.F.\mu_o}{\pi}\left(\frac{2}{r_c} + \frac{V_x}{r_c^2} + \frac{4.t}{r_a^2}\right)\left(\frac{0.2\,T_m}{T_m - T_o}\right) \qquad (21)$$

Figure 7 shows the variation in heat flux with the dimensionless numbers.

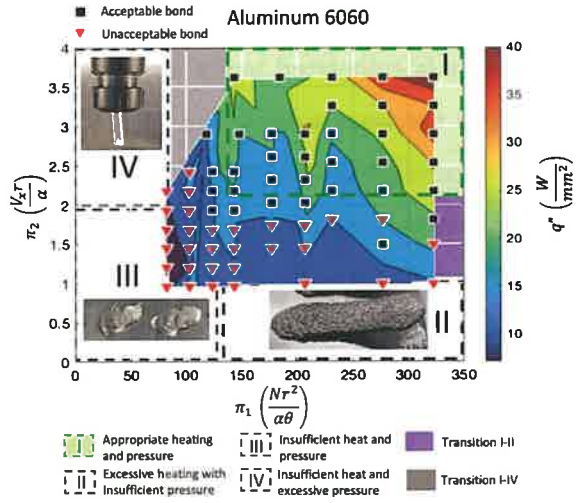

Figure 7. Variation of heat flux with dimensionless numbers

A.1.4.3 Practical applications of the methodology

The pressure variation provides a guide to users for the selection of appropriate parameters to achieve sound friction surfacing deposits. Currently, the initial parameter matrix for friction surfacing is chosen based on a literature survey or hit and trial bases. The dimensionless numbers provided in this study can allow users to select starting parameters. For example, based on the application, the user has the alloy properties $(\alpha,\ \theta, and\ \sigma_y)$. Based on the application or final product requirement, the appropriate rod size (r) is selected. Using these parameters, the user can select the appropriate π_1 and π_2 values. The pressure field in the plots is also helpful for knowing if the equipment can successfully take the axial loads during the process. The plot not just helps in the selection of the appropriate parameter but also provides a guide to adjust the parameters if the coatings are not acceptable (Region 'II-IV').

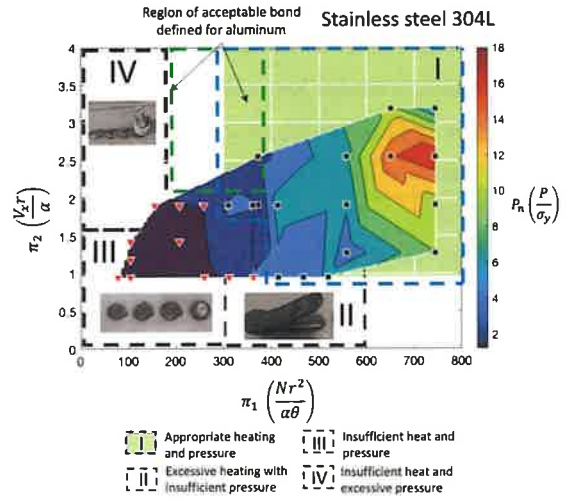

Figure 8. Validation of trends with stainless steel 304L

A.1.5 Conclusions

This study presents a novel approach to finding processing regimes during friction surfacing. Two dimensionless numbers consisting of the processing parameters and thermomechanical properties of the consumable rod are used to identify processing regions that produce deposits with strong bonding. Through these dimensionless numbers and process maps, a new user will be able to select appropriate processing parameters for a given application (resolution, material, and machinery). The study also identifies possible unacceptable regimes during friction surfacing and provides insights into adjusting the processing parameters for achieving acceptable deposits.

References

[1] J. Gandra, H. Krohn, R. M. Miranda, P. Vilaça, L. Quintino, and J. F. dos Santos, "Friction surfacing - A review," Journal of Materials Processing Technology, vol. 214, no. 5. Elsevier Ltd, pp. 1062–1093, 2014. doi: 10.1016/j.jmatprotec.2013.12.008.1

[2] Gandra, J., R. M. Miranda, and P. Vilaça. "Performance analysis of friction surfacing." Journal of Materials Processing Technology 212, no. 8 (2012): 1676-1686.

[3] V. I. Vitanov, N. Javaid, and D. J. Stephenson, "Application of response surface methodology for the optimisation of micro friction surfacing process," Surface and Coatings Technology, vol. 204, no. 21–22, pp. 3501–3508, Aug. 2010, doi: 10.1016/j.surfcoat.2010.04.011.

[4] Voutchkov, I., B. Jaworski, V. I. Vitanov, and G. M. Bedford. "An integrated approach to friction surfacing process optimisation." Surface and coatings technology 141, no. 1 (2001): 26-33.

[5] Chandrasekaran, Margam, Andrew William Batchelor, and Sukumar Jana. "Friction surfacing of metal coatings on steel and aluminum substrate." Journal of Materials Processing Technology 72, no. 3 (1997): 446-452.

Appendix (data)

Test no.	Diameter of the rod (mm)	Spindle speed, N (RPM)	Traverse feed rate, V_x (mm/min)	Axial feed rate, V_z (mm/min)	Bond quality (Peel -off test)	π1 ($Nr^2/\alpha\Theta$)	π2 ($Vx\ r/\alpha$)	Axial force, F (N)	Width of the coating, w (mm)	Thickness of the coating, t (mm)	Contact radius, r_c (mm)	Diameter of flash, d_f (mm)	Axial pressure, P (Mpa)	Total haet flux, q (W/mm^2)
1	10	4000	1000	550	unacceptable	82	1.21	891	13.4	2.7	0.0046	16	13.6	7.04E+06
2	10	4000	1200	660	unacceptable	82	1.45	1037	14.3	2.82	0.0048	17	14.1	7.72E+06
3	10	4000	1400	770	unacceptable	82	1.69	1113	13.8	2.68	0.0046	18	16.6	8.21E+06
4	10	4000	1600	880	unacceptable	82	1.93	1224	14.1	2.79	0.0048	17	17.1	9.17E+06
5	10	4000	1800	990	unacceptable	82	2.17	1364	13.9	2.59	0.0046	17	20.8	1.04E+07
6	10	4000	800	440	unacceptable	82	0.97	900	13.4	1.98	0.0039	18	18.7	7.14E+06
7	10	5000	800	440	unacceptable	103	0.97	2100	20.4	2.59	0.0055	17	21.9	1.73E+07
8	10	5000	1000	550	unacceptable	103	1.21	1008	12.8	2.55	0.0043	17	17.0	9.88E+06
9	10	5000	1200	660	unacceptable	103	1.45	1147	14.1	2.59	0.0046	17	17.3	1.08E+07
10	10	5000	1400	770	unacceptable	103	1.69	1273	13.1	2.18	0.0041	17	24.5	1.27E+07
11	10	5000	1600	880	unacceptable	103	1.93	1392	11.5	3.5	0.0048	17	19.0	1.38E+07
12	10	5000	1800	990	acceptable	103	2.17	1778	14.6	2.36	0.0045	17	28.4	1.68E+07
13	10	5000	2000	1100	unacceptable	103	2.41	1568	14.5	2.35	0.0044	17	25.3	1.49E+07
14	10	6000	800	440	unacceptable	123	0.97	804	12.7	3.25	0.0049	17	10.7	9.25E+06
15	10	6000	1000	550	unacceptable	123	1.21	1008	12.6	2.97	0.0047	17	14.8	1.17E+07
16	10	6000	1200	660	unacceptable	123	1.45	1147	13.4	2.82	0.0047	17	16.7	1.31E+07
17	10	6000	1400	770	unacceptable	123	1.69	1300	15.8	2.21	0.0045	17	20.5	1.44E+07
18	10	6000	1600	880	acceptable	123	1.93	1211	11.6	2.73	0.0043	17	21.0	1.47E+07
19	10	6000	1800	990	acceptable	123	2.17	1283	15.6	2.31	0.0046	17	19.6	1.42E+07
20	10	6000	2000	1100	acceptable	123	2.41	1577	14.2	2.29	0.0043	17.3	26.7	1.80E+07
21	10	7000	800	440	unacceptable	144	0.97	839	12.3	2.78	0.0044	17	13.5	1.15E+07
22	10	7000	1000	550	unacceptable	144	1.21	1009	12.4	2.43	0.0042	17	18.4	1.41E+07
23	10	7000	1200	660	unacceptable	144	1.45	1171	12.5	2.34	0.0041	17	22.0	1.64E+07
24	10	7000	1400	770	unacceptable	144	1.69	1309	12.7	2.31	0.0041	17	24.5	1.83E+07
25	10	7000	1600	880	acceptable	144	1.93	1394	13.1	2.61	0.0044	17	22.4	1.89E+07
26	10	7000	1800	990	acceptable	144	2.17	1381	16.4	2.2	0.0046	15.4	21.1	1.85E+07
27	10	7000	2000	1100	acceptable	144	2.41	1604	12.7	2.1	0.0039	16	33.1	2.35E+07
28	10	7000	3000	1650	acceptable	144	3.62	2004	14.4	2.31	0.0044	17.5	33.1	2.65E+07
29	12	4000	2000	1100	acceptable	118	2.90	2507	20.4	2.59	0.0055	22.1	26.1	1.46E+07
30	12	5000	2000	1100	acceptable	148	2.90	2585	18.1	2.57	0.0052	22.3	30.6	1.98E+07
31	12	6000	1000	550	unacceptable	177	1.45	1475	15.5	3.4	0.0055	23.7	15.4	1.32E+07
32	12	6000	1200	660	unacceptable	177	1.74	1625	16.3	3	0.0053	23.7	18.3	1.47E+07
33	12	6000	1400	770	acceptable	177	2.03	1930	17.4	2.74	0.0053	23.3	22.3	1.74E+07
34	12	6000	1600	880	acceptable	177	2.32	2040	17.2	2.65	0.0051	23.6	24.6	1.86E+07
35	12	6000	1800	990	acceptable	177	2.61	2050	19.8	2.5	0.0054	22.6	22.8	1.81E+07
36	12	6000	2000	1100	acceptable	177	2.90	2593	17.7	2.37	0.0049	24.3	34.0	2.39E+07
37	12	6997	1000	550	unacceptable	207	1.45	1434	14.4	3.26	0.0052	24.1	16.8	1.55E+07
38	12	6997	1200	660	unacceptable	207	1.74	1612	15.2	2.68	0.0049	25	21.8	1.77E+07
39	12	6997	1400	770	acceptable	207	2.03	1903	16.6	2.54	0.0049	24.8	24.8	2.04E+07
40	12	6997	1600	880	acceptable	207	2.32	1956	17.8	2.63	0.0052	23.8	23.0	2.05E+07
41	12	6997	1800	990	acceptable	207	2.61	1960	15.9	2.1	0.0044	25	32.3	2.28E+07
42	12	7000	690	379.5	unacceptable	207	1.00	1098	13.8	3.8	0.0055	24.6	11.5	1.16E+07
43	12	7000	2000	1100	acceptable	207	2.90	2600	16.1	1.94	0.0043	25.2	45.8	3.09E+07
44	15	4000	2000	1100	acceptable	185	3.62	3984	20.2	2.22	0.0051	26.4	48.9	2.31E+07
45	15	5000	1000	550	unacceptable	231	1.81	2382	19.7	3.45	0.0063	29.4	19.3	1.49E+07
46	15	5000	1200	660	acceptable	231	2.17	2670	21.3	3.06	0.0061	29.9	22.5	1.66E+07
47	15	5000	1400	770	acceptable	231	2.54	2838	21.7	2.96	0.0061	28.9	24.3	1.78E+07
48	15	5000	1600	880	acceptable	231	2.90	3270	20.8	2.91	0.0059	30.1	29.7	2.08E+07
49	15	5000	1800	990	acceptable	231	3.26	3635	21.5	2.2	0.0052	29	42.3	2.52E+07
50	15	5000	2000	1100	acceptable	231	3.62	3865	20.7	2.44	0.0054	28.6	42.1	2.64E+07
51	15	6000	550	302.5	unacceptable	277	1.00	1579	15.7	3.69	0.0058	29.3	15.0	1.28E+07
52	15	6000	830	456.5	acceptable	277	1.50	2165	16.8	3.72	0.0060	27.8	19.1	1.73E+07
53	15	6000	1000	550	unacceptable	277	1.81	2572	19.2	3	0.0058	29.6	24.6	2.02E+07
54	15	6000	1200	660	acceptable	277	2.17	2785	20	2.56	0.0054	29.2	29.9	2.26E+07
55	15	6000	1400	770	acceptable	277	2.54	3111	21.6	3	0.0061	28.4	26.4	2.35E+07
56	15	6000	1600	880	acceptable	277	2.90	3333	21.3	2.63	0.0057	29.4	32.7	2.61E+07
57	15	6000	1800	990	acceptable	277	3.26	3520	21.6	2.1	0.0051	28.6	42.7	2.97E+07
58	15	6000	2000	1100	acceptable	277	3.62	4031	17.5	1.93	0.0044	28.1	65.6	3.89E+07
59	15	7000	550	302.5	unacceptable	323	1.00	1555	14.7	4.24	0.0060	28.9	13.7	1.47E+07
60	15	7000	830	456.5	unacceptable	323	1.50	2093	17.4	2.5	0.0050	29.5	26.5	2.12E+07
61	15	7000	1000	550	acceptable	323	1.81	2475	18	2.66	0.0053	29.4	28.4	2.42E+07
62	15	7000	1200	660	acceptable	323	2.17	2804	19.3	2.19	0.0049	29	36.5	2.85E+07
63	15	7000	1400	770	acceptable	323	2.54	2994	19	2.2	0.0049	29.6	39.4	3.05E+07
64	15	7000	1600	880	acceptable	323	2.90	3540	21.9	1.75	0.0047	29.3	50.8	3.70E+07
65	15	7000	1800	990	acceptable	323	3.26	3278	20.9	1.74	0.0046	29.5	49.6	3.51E+07
66	15	7000	2000	1100	acceptable	323	3.62	3697	15.8	1.84	0.0041	28.6	69.9	4.43E+07

to produce deposits with near-wrought properties. Additionally, solid-state additive processes reduce the overall embodied energy to reuse machining chips. Agrawal *et al.* [6] successfully used recycled Ti-6Al-4V in an additive friction stir deposition process. The deposited parts exhibited tensile properties better than other additive processes. Researchers have also studied friction stir extrusion to produce wires from machining chips [9], [10]. It was assessed that full density and high mechanical properties products can be obtained from machined scraps of different light alloys.

Friction surfacing is one such friction-based solid-state process that can potentially use metal cutting chips as a feedstock. It is a solid-state deposition process where a rotating consumable tool is pressed against a substrate under an applied axial load. The frictional heat generated at the contact plastically deforms the tool material, which is subsequently traversed over the substrate to produce a deposition. The intense plastic straining of the material leads to dynamic recrystallization in the deformed material, leading to depositions with superior mechanical and corrosion properties compared to the fusion-based processes. A schematic of the process can be seen in Figure 1Error! Reference source not found.. While friction surfacing is primarily used for coating surfaces to improve their wear properties, it is also showing promising results as an additive manufacturing process for repair / remanufacturing features on large metal parts. Karthik *et al.* [11] deposited multiple layers of aluminum matrix composite reinforced with consolidating titanium particles using friction surfacing tools. Intermetallic bands were formed at the interface, which strongly affected the ductility of the multilayer build. In a similar multilayer fashion, Gandra *et al.* [12] deposited Aluminum-SiC depositions to create a functionally graded build. They employed several strategies with respect to hole diameter, location, and the number of holes to fill SiC in friction surfacing tools. They reported a 30% increase in surface hardness in depositions with reinforcement particles. In this work, we propose the direct reuse of metal cutting chips as a feedstock for the friction surfacing process.

The motivation of this research is to improve the understanding and implementation of circular manufacturing to reduce energy consumption, reduce cost, and increase resource efficiency. To the author's knowledge, it is the first study to employ friction surfacing as a potential method of reusing metal cutting chips. Friction surfaced depositions were deposited using stainless steel 304L consumable tools embedded with 316L metal cutting chips. The deposition morphology, process efficiency, and bonding strength of the depositions have been discussed.

Table 1: Chemical composition

Element (Wt %)	C	Mn	P	S	Si	N	Cr	Ni	Mo	Cu	Fe
Substrate (304L)	0.015	1.74	0.031	0.001	0.273	0.094	18.01	8.061	0.373	0.467	Balance
Consumable tool (304L)	0.02	1.68	0.033	0.028	0.33	0.082	18.23	8.09	0.2	0.56	Balance
Metal cutting chips (316L)	0.018	1.44	0.012	0.028	0.53	0.068	16.6	10.6	2.24	0	Balance

Table 2: Process parameters used in this study

Tool outer diameter, D_o	12.7 mm
Hole diameter, D_i	0, 4.76, 6.35, 7.14 mm
Spindle rotation speed, N	4000 rpm
Transverse feed rate, V_x	90, 120 mm/min
Velocity ratio, V_z/V_x	0.4

The axial feed rate (Vz) was appropriately chosen to keep a constant velocity ratio (Vz/Vx) of 0.4. Table 2 summarizes the tool dimensions and process parameters for the friction surfacing process. The workpieces were mounted atop a three-axis piezoelectric force dynamometer (Kistler model 9285), which measured the transient process forces. Friction surfacing deposits and tools were cross-sectioned in the steady state region to analyze the process and properties of the deposit. Deposition morphology, i.e., total width (W), bonded width (B) and thickness (T) were analyzed using a white light optical metrology system (Alicona, InfiniteFocus® G4, Austria).

Lichtenegger-Bloech (LBI) etchant (100 mL distilled water; 20 g ammonium hydrogen difluoride 0.5–1 g potassium disulfite; heated to 37 °C) was used to add color to the images. Etched samples were then imaged using the white light optical metrology system. The deposition efficiency of the process was calculated using the measured total width (W) and thickness (T). The formula of deposition efficiency ($\eta_{Deposition}$) and bonded efficiency (η_{Bonded}) are given as equation (1) and (2). The formula accounts for the density of the consolidated chips, which is approximated by the volume of the inner blind hole and weight of the consolidated chips.

$$\eta_{Deposition} = \frac{WTV_x}{\left(\frac{\pi D_i^2}{4}\rho_{chips} + \frac{\pi}{4}\left(D_o^2 - D_i^2\right)\right)V_z} \quad \text{(Equation 1)}$$

$$\eta_{Bonded} = \frac{WTV_x}{\left(\frac{\pi D_i^2}{4}\rho_{chips} + \frac{\pi}{4}\left(D_o^2 - D_i^2\right)\right)V_z} \times \frac{B}{W} \quad \text{(Equation 2)}$$

Here, ρ_{chips} is the relative density of the chips.

Room temperature tensile test were performed on a universal testing machine (MTS®, Sintech, USA) load frame with a 50 kN load cell and 2.20 mV/V sensitivity in accordance with the ASTM E8 standard. Tests were carried out at a constant crosshead rate of 5 mm/min (strain rate of 0.1 s). Acquired stress-strain data was then used to analyze the Ultimate tensile strength (UTS), Yield strength (Y), Fracture strength (F), and elongation (%) of the coated samples.

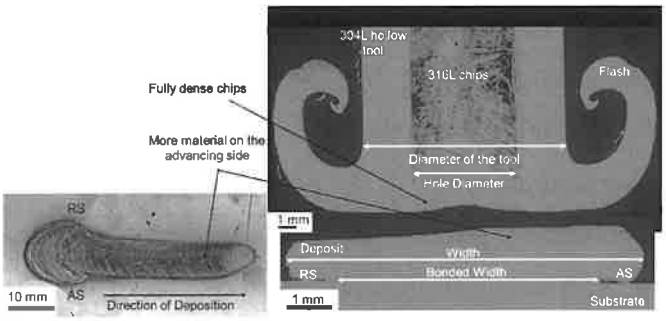

Figure 2: (a) Coating with chip filled rod (b) cross section of the chip filled rod and tool

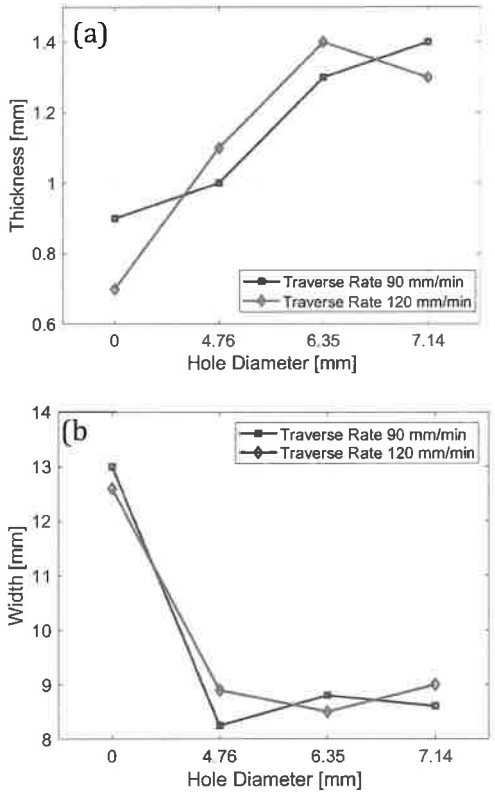

Figure 3: (a) Coating Thickness Vs. Hole diameter (b) Coating width Vs. Hole diameter

There is more material deposited on the advancing side (rotation and travel movements are in the same direction) of the deposition compared to the retreating side, as shown in Figure 2. Also, overall friction surfaced depositions were observed to be leaning towards the advancing side, which is due to the combined effect of rotation and travel speed on a plastically deformed layer not constrained around the tool [add reference]. The surface of the depositions made with the chip-filled tool shows a circular or elliptical pattern on the surface that is generally observed in friction surfacing depositions.

A.2.3.2 Process Forces

Figure 5 shows the comparison of the measured axial force for solid 304L, solid 316L, and tools filled with 316L chips deposited using the same process parameters. The process is divided into two phases, the pre-heating phase, where frictional heating dominates the process, and the consumable tool is getting plastically deformed. Once the entire rod surface gets plastically deformed, the process enters a steady-state plastic deformation phase. The pre-heating zone experiences the highest force at the beginning, as the rotating tool is plunged into the cold substrate. This plunging force was found to be reduced in the tool that is filled with chips. The steady-state forces are also reduced and show reduced fluctuations for chip-filled tools, indicating smoother material flow or improved damping during the process. Figure 5 b shows that axial force decreases with increasing inner hole diameter i.e., a greater volume of metal cutting chips and thinner tool wall. It was also observed that coatings produced with solid 316L tools with same set of process parameters did not produce uniform consolidated deposition. Successful 316L deposition was achieved by reducing the transverse feed rate. Lowered axial forces measured during the process support the observations made in the morphology of the deposition. The increased thickness and reduced width with growing unbonded regions of the depositions indicate insufficient forces develop at the tip of the rod with increasing the hole diameter of consolidated chips. Hence, the axial feed rate needs adjustment with increasing hole diameter in the chip consolidated rod to achieve improved performance.

Table 3: Coatings process variables

	Process Parameters		Deposit Morphology			Efficiency		Forces
Sample Number	Tool inner hole diameter, D_i (mm)	Transverse Feed rate, V_x (mm/min)	Total Width, W (mm)	Bonded Width, B (mm)	Thickness, T (mm)	Deposition Efficiency (%)	Bonded Deposition Efficiency (%)	Average Axial Force (N)
1	0	90	13.0	10.0	0.8	22.6%	17.4%	6000
2	0	120	12.6	10.0	0.7	18.2%	14.4%	8500
3	4.76	90	8.3	5.8	1.0	17.6%	5.8%	3800
4	4.76	120	8.8	5.6	1.0	19.3%	12.1%	4800
5	6.35	90	8.8	5.8	1.3	23.4%	14.5%	2800
6	6.35	120	8.5	6.2	1.4	24.8%	12.5%	4000
7	7.14	90	8.6	4.2	1.4	24.4%	10%	2600
8	7.14	120	9.0	4.2	1.3	24.1%	11.4%	3800

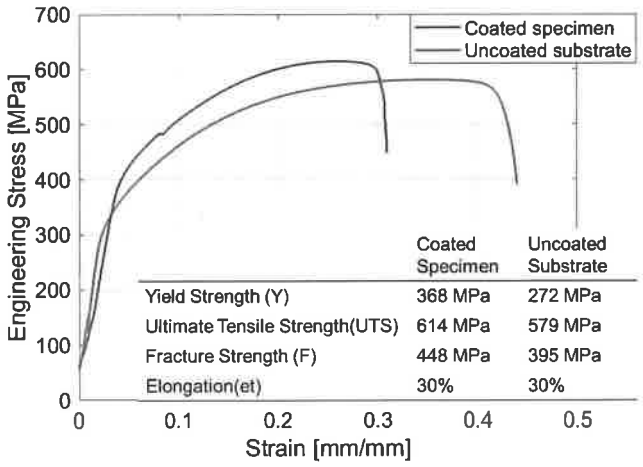

Figure 6: Tensile Properties of coated and uncoated substrate

A.2.3.4 Material flow

Figure 7 show cross-sectional images after etching the specimen with Lichtenegger-Bloech (LBI) etchant. LBI etchant is used to highlight different phases in the stainless steel. The rate of etching in different phases helps distinguish them from each other. The LBI etchant can also be used to distinguish different grades of austenitic stainless steels owing to their varied corrosion resistance. Stainless steel 316L is known for its higher corrosion properties compared to stainless steel 304L due to the presence of molybdenum. Hence, between the two materials, 304L shows faster discoloration in the etchant solution. For depositions with chip filled tool, higher discoloration of the substrate compared to depositions indicate most regions of deposition consist of stainless steel 316L; which means depositions are mostly comprised of metal cutting chips. In friction surfaced rods, material flow if the machining chips can be observed. While in friction surfaced tools, discoloration of the flash is observed which suggest the 304L from the shell of the rod roll up in the flash during the process. Similar results were noted by Fukakusa [15], where material flow in the friction surfacing process was studied by compressing filler rod in the hollow tool of different material. The Rod with Φ4.76 hole diameter (Figure 7) reveals that all the chips have moved down to the deposition and a straight hole profile is still maintained, while the rod with Φ7.16 hole diameter shows that machining chips have also rolled out in the flash. This suggests that a hole diameter can be chosen where all chips are reused in the depositions maintaining the uniform chemical composition without losses through the flash. A detailed investigation will be performed in future work where material flow during the process and microstructural evolution of the chips to depositions will be investigated.

[4] B. Fullenwider, P. Kiani, J. M. Schoenung, and K. Ma, "Two-stage ball milling of recycled machining chips to create an alternative feedstock powder for metal additive manufacturing," Powder Technology, vol. 342, pp. 562–571, Jan. 2019, doi: 10.1016/j.powtec.2018.10.023.

[5] K. Mahmood, W. U. H. Syed, and A. J. Pinkerton, "Innovative reconsolidation of carbon steel machining swarf by laser metal deposition," Optics and Lasers in Engineering, vol. 49, no. 2, pp. 240–247, Feb. 2011, doi: 10.1016/j.optlaseng.2010.09.014.

[6] P. Agrawal et al., "Processing-structure-property correlation in additive friction stir deposited Ti-6Al-4V alloy from recycled metal chips," Additive Manufacturing, vol. 47, p. 102259, Nov. 2021, doi: 10.1016/j.addma.2021.102259.

[7] J. W. Murray, A. Speidel, A. Jackson-Crisp, P. H. Smith, H. Constantin, and A. T. Clare, "Unprocessed machining chips as a practical feedstock in directed energy deposition," International Journal of Machine Tools and Manufacture, vol. 169, p. 103803, Oct. 2021, doi: 10.1016/j.ijmachtools.2021.103803.

[8] F. Khodabakhshi and A. P. Gerlich, "Potentials and strategies of solid-state additive friction-stir manufacturing technology: A critical review," Journal of Manufacturing Processes, vol. 36, pp. 77–92, Dec. 2018, doi: 10.1016/j.jmapro.2018.09.030.

[9] D. Baffari, G. Buffa, D. Campanella, and L. Fratini, "Design of continuous Friction Stir Extrusion machines for metal chip recycling: issues and difficulties," Procedia Manufacturing, vol. 15, pp. 280–286, Jan. 2018, doi: 10.1016/j.promfg.2018.07.220.

[10] W. Tang and A. P. Reynolds, "Production of wire via friction extrusion of aluminum alloy machining chips," Journal of Materials Processing Technology, vol. 210, no. 15, pp. 2231–2237, Nov. 2010, doi: 10.1016/j.jmatprotec.2010.08.010.

[11] G. M. Karthik, G. D. J. Ram, and R. S. Kottada, "Friction deposition of titanium particle reinforced aluminum matrix composites," Materials Science and Engineering: A, vol. 653, pp. 71–83, Jan. 2016, doi: 10.1016/j.msea.2015.12.005.

[12] J. Gandra, P. Vigarinho, D. Pereira, R. M. Miranda, A. Velhinho, and P. Vilaça, "Wear characterization of functionally graded Al–SiC composite coatings produced by Friction Surfacing," Materials & Design (1980-2015), vol. 52, pp. 373–383, Dec. 2013, doi: 10.1016/j.matdes.2013.05.059.

[13] H. K. Rafi, G. D. J. Ram, G. Phanikumar, and K. P. Rao, "Friction surfaced tool steel (H13) coatings on low carbon steel: A study on the effects of process parameters on coating characteristics and integrity," Surface and Coatings Technology, vol. 205, no. 1, pp. 232–242, Sep. 2010, doi: 10.1016/j.surfcoat.2010.06.052.

[14] H. Agiwal, H. Yeom, K. A. Ross, K. Sridharan, and F. E. Pfefferkorn, "Leak-tight crack repair for 304L stainless steel using friction surfacing," Journal of Manufacturing Processes, vol. 79, pp. 532–543, Jul. 2022, doi: 10.1016/j.jmapro.2022.05.004.

[15] K. Fukakusa, "On the characteristics of the rotational contact plane - a fundamental study of friction surfacing," Welding International, vol. 10, no. 7, pp. 524–529, Jan. 1996, doi: 10.1080/09507119609549043.